OPEN

A Highly Efficient Hybrid GaAs Solar Cell Based on Colloidal-Quantum-Dot-Sensitization

Hau-Vei Han[1], Chien-Chung Lin[2], Yu-Lin Tsai[1], Hsin-Chu Chen[1,3], Kuo-Ju Chen[1], Yun-Ling Yeh[1], Wen-Yi Lin[1], Hao-Chung Kuo[1] & Peichen Yu[1]

[1]Department of Photonics and Institute of Electro-Optical Engineering, National Chiao Tung University, Hsinchu 30010, Taiwan, [2]Institute of Photonic System, National Chiao Tung University, Tainan 711, Taiwan, [3]Electronics and Optoelectronics Research Laboratories, Industrial Technology Research Institute, Hsinchu 30010, Taiwan.

This paper presents a hybrid design, featuring a traditional GaAs-based solar cell combined with various colloidal quantum dots. This hybrid design effectively boosts photon harvesting at long wavelengths while enhancing the collection of photogenerated carriers in the ultraviolet region. The merits of using highly efficient semiconductor solar cells and colloidal quantum dots were seamlessly combined to increase overall power conversion efficiency. Several photovoltaic parameters, including short-circuit current density, open circuit voltage, and external quantum efficiency, were measured and analyzed to investigate the performance of this hybrid device. Offering antireflective features at long wavelengths and luminescent downshifting for high-energy photons, the quantum dots effectively enhanced overall power conversion efficiency by as high as 24.65% compared with traditional GaAs-based devices. The evolution of weighted reflectance as a function of the dilution factor of QDs was investigated. Further analysis of the quantum efficiency response showed that the luminescent downshifting effect can be as much as 6.6% of the entire enhancement of photogenerated current.

Among various solar cell technologies, GaAs-based solar cells have become important because of their high power conversion efficiency (PCE). GaAs-based single-junction solar cells have recently achieved PCEs of 28.8%, setting new photovoltaic efficiency records[1–4]. In addition to reducing surface reflection[5,6], using the full solar spectrum is necessary for increasing PCE further, especially the ultraviolet (UV) range. High-energy photons can be easily absorbed at short distances, but the generated electron-hole pairs are close to the semi-conductor surface, where recombination loss is strong[7]. This problem can be mitigated using certain substances to transform high-energy photons into lower-energy photons; this process is often called luminescent downshifting (LDS). In the 1970s, Hovel et al. first reported that the LDS effect could enhance solar cell performance at short wavelengths[8]. Certain studies have examined the use of organic dyes as downshifters[9–11]. However, organic dye molecules have poor photon stability and narrow absorption spectrum bands, and obtaining high PCE by using organic dye molecules is difficult[12,13]. One possible solution is to use semiconductor-based quantum dots (QDs, or sometimes called colloidal quantum dots, QDs), such as CdS or CdSe, in the regular solar cell[14–16]. These QDs can act as the LDS agents to initiate UV absorption and boost the power conversion efficiency of the solar cell. Considering current advances in QD preparation and manufacturing, these highly efficient nanoscale luminaries offer an unprecedented opportunity to advance solar spectrum use where previous research has failed[17–19]. In the past, many excellent experiments and theoretical works related to spectral response of LDS materials have been published for the photovoltaic devices, especially in the dye-sensitized or thin film types of solar cells[9,20–28]. Recent researches benefit from the advanced progress in the synthesis of highly efficient QDs. The application of these novel materials leads to great enhancement, such as a 3% to 28% increase of J_{sc}, among different types of semiconductor solar cell (such as Si or CdTe)[29,30]. In theory, this improvement can be as high as 50%[31]. These demonstrations in experiment or in theory really established the prominent role of the QD-assisted LDS effect for the next generation of photovoltaic devices. In our work, the direct surface dispense of QD layers on GaAs solar cell is investigated under different emission wavelengths, and the device performance is studied in details. A practical formulation is set up to have good estimate on the LDS effect. QD band-gap dependent photovoltaic responses were analyzed, and the quantities of QDs necessary to obtain optimal PCEs were identified using external quantum efficiency and current density-voltage (J-V) characteristics.
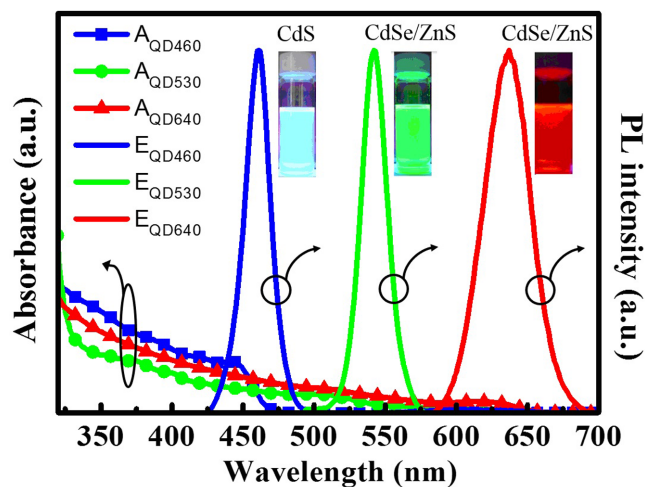
Figure 1 | UV-Visible absorbance and photoluminescence (blue, green, and red) spectra of QDs measure in toluene. The PLE spectrum was taken at the maximum of PL intensity (460 nm, 530 nm, and 640 nm). For the PL spectrum, the sample was excited by a light beam with 365 nm. The insets are the photos of quantum dot solution under UV excitation.

Results

Different types of QD were obtained from the Sigma-Aldrich Corporation for this experiment. Photoluminescence (PL) and absorption spectra were measured to determine the optical characteristics of the QDs (as shown in Fig. 1). The PL emission spectra of three types of QD in toluene were measured using a 365-nm excitation, and showed different peaks at 460 nm, 530 nm, and 640 nm. Regarding the chemical composition of the QDs, CdS was used for emission wavelengths shorter than 460 nm, and CdSe/ZnS core-shell was used for emission wavelengths longer than 530 nm[32].

Fig. 2 shows the process flow used to create the QD-sensitized single-junction GaAs solar cell. The single-junction GaAs solar cells were manufactured by Millennium Communications Co. Ltd., and QD sensitization was performed following procedures described previously[15]. The back-side n-contact in the proposed design was formed by evaporating AuGe (25 nm)/Au (500 nm), whereas the front p-contact consisted of evaporated Ti (25 nm)/Pt (25 nm)/Au (500 nm). The shadow loss of the front strip contacts was 3.5%, and area of the cells was 1 cm². The QD solutions were dispensed by the procedures described in the "Method" section to get ready for the IV and EQE measurements.

Fig. 3(a) shows a scanning electron microscopy (SEM) image, taken from the top view at a 45° tilt, of QDs on the GaAs solar cell surface. Because of the self-assembly effect, individual QDs gather together after the solvent dries up to form submicron islands. Although grain sizes were randomly distributed, most grain dia-
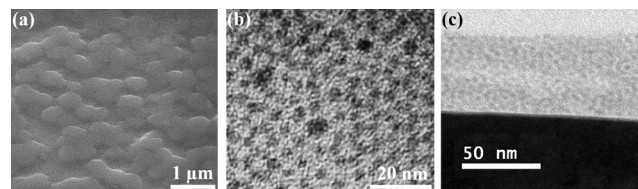

Figure 3 | (a) 45° tilted top view of SEM image of self-assembly QDs on the GaAs solar cell surface. (b)(c) TEM images of QDs are shown.

meters ranged from 100 to 500 nm, and grain thicknesses were approximately several tens of nanometers. Fig. 3(b) shows a transmission electron microscopy (TEM) image of the QDs with a 460 nm emission peak. Each QD had a diameter of approximately 5 nm in 460-nm QD solution, and exhibited a uniform density distribution. Moreover, the emission peak was tunable based on the diameters of the QDs. When the QD particles were larger in size, the emission peak wavelength was redshifted. The average diameter of 530-nm QDs and 640-nm QDs were approximately 6 nm and 8 nm, respectively. Fig. 3(c) shows the cross-sectional view of a QD grain, and random stacking of dots can be found. After the colloidal QDs were dispensed onto the GaAs solar cell surfaces, we measured device characteristics such as photovoltaic current density-voltage (J-V) and external quantum efficiency (EQE).

To map the spectral dependence, five colors of QDs were used, and a QD concentration of 5 mg/mL was applied in each case for the first test run. Fig. 4(a) shows the short-circuit current density results of cells with and without QDs. The x axis indicates the emission peak of the specific QD dispensed onto the GaAs cell.

As shown in Fig. 4(a), all devices with QDs exhibited higher J_{sc} than devices without QDs (the reference sample). The short-circuit current response peaks at 530 nm, and in general, the QD with shorter wavelengths (such as 400 nm and 460 nm) performs better than the longer ones (like those of 560 nm and 640 nm QDs). Because the quantum yield of each QD can differ, and GaAs solar cell responses vary at different wavelengths, the spectral dependence can be qualitatively described as follows. When QD emission wavelengths were shorter (such as blue or purple), the corresponding quantum efficiency of the GaAs solar cell was fair (generally, approximately 30% to 40%), but not as high as that of longer wavelength regions (70% to 80% between green and red). The enhancement of J_{sc} was expected to increase as the applied QD emission wavelength moved toward the longer side of spectrum. However, as the emission wavelength moves past the green and enters the orange and red regions in Fig. 4(a), the interference of QD absorption must also be considered. As shown in Fig. 1, the absorption edges of these QDs are close to their emission peaks. When red QDs are used, this absorption could affect the normal GaAs absorption between UV and yellow. Because the QD absorption and reemission mechanism is not as efficient as that in regular semiconductors, which
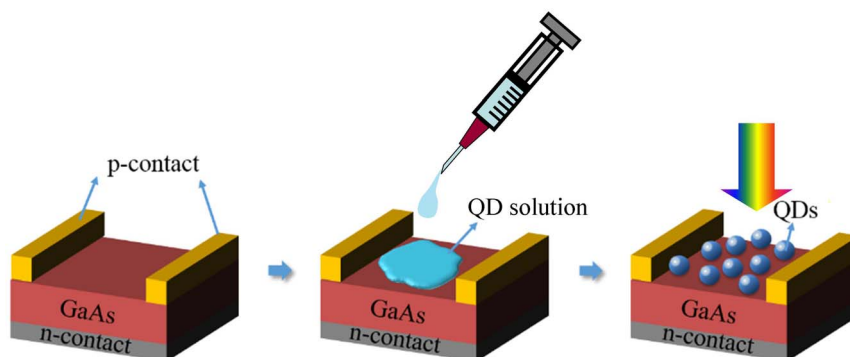

Figure 2 | The process flow of the QD-sensitized single-junction GaAs solar cell.
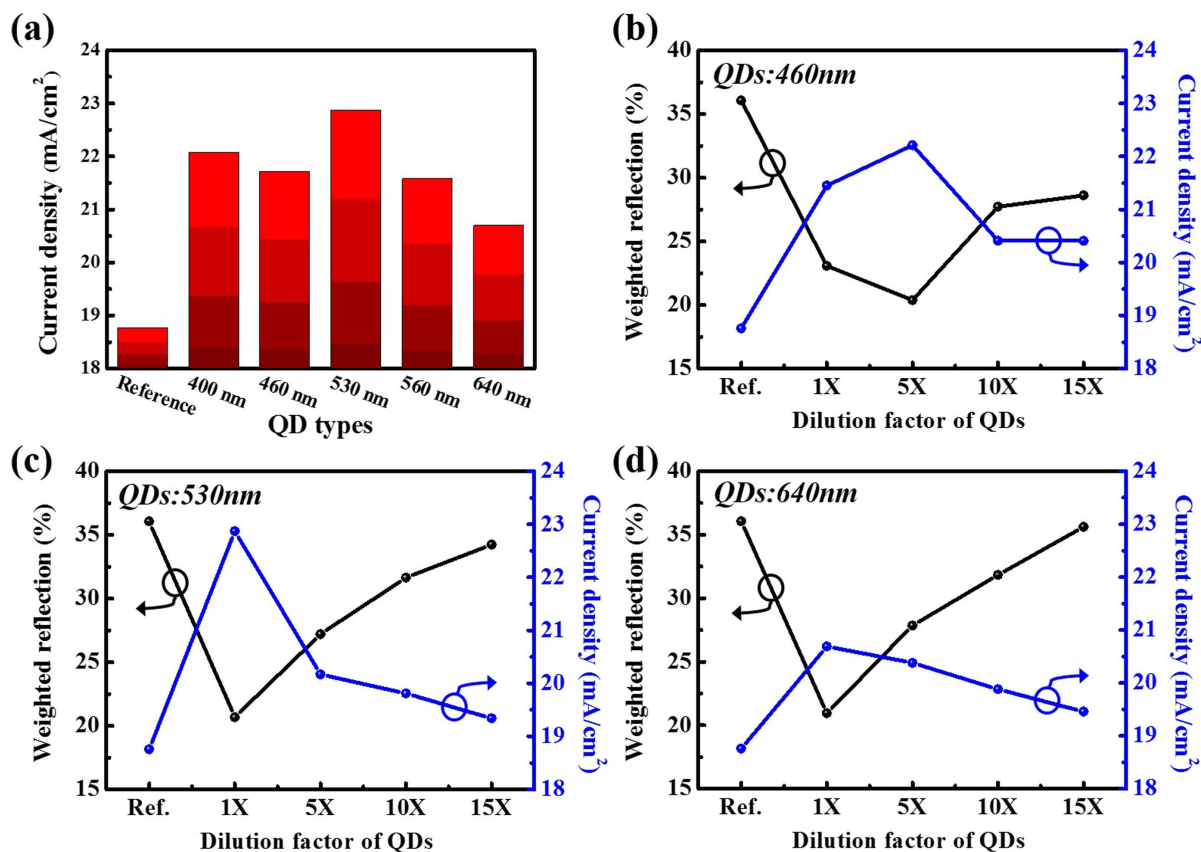
Figure 4 | (a) Evolution of short-circuit current density as a function of QD emission wavelength of 400 nm QDs, 460 nm QDs, 530 nm QDs, 560 nm QDs and 640 nm QDs on GaAs solar cells. Evolution of weighted reflectance and short-circuit current density as a function of the dilution factor of (b) 460 nm QDs, (c) 530 nm QDs, and (d) 640 nm QDs on GaAs solar cells.

operate in the more visible range covered by QD absorption, less carriers are generated because of less visible photons into GaAs. In our experiments shown in Fig. 4(a), the composite effects of LDS and absorption-takeover meet at the wavelength of 530 nm.

Based on our results in Fig. 4(a), three QDs were used for more detailed experiments; the maximum wavelength (530 nm) and two adjacent wavelengths of QDs (460 nm and 640 nm) were used to investigate the concentration-dependent response. Using the dilution factor "1×," a concentration of 5 mg/mL of QD solution was dispensed directly onto the surface of a GaAs solar cell; "5×" was 1 mg/mL, "10×" was 0.5 mg/mL, "15×" was 0.33 mg/mL, and the "Reference" was zero QDs on the solar cell. When QDs were applied to the GaAs surface, as thin as several tens of nanometer (shown in Fig. 3), a considerable reduction in surface reflectance was observed because of its intermediate refractive index ($n \approx 2.4$) and photon-scattering capability[33,34]. As QD solution concentration increased, the surface reflectance was reduced. To compare samples using different dilution factors in the same terms, solar-spectrum weighted reflectance was defined to express the antireflective power of the nanostructures as the following[35,36]:

$$\langle R \rangle = \frac{\int_{300nm}^{1000nm} I_{AM1.5G}(\lambda) \times R(\lambda)d\lambda}{\int_{300nm}^{1000nm} I_{AM1.5G}(\lambda)d\lambda} \quad (1)$$

where R (λ) is the measured reflectivity and $I_{AM1.5}$ is the photon flux density of the AM1.5G solar spectrum. Weighted reflectance using different dilution factors (1×, 5×, 10×, and 15×) was calculated based on the measurements. As shown in Figs. 4(b) to 4(d), weighted reflectance and J_{sc} are plotted against different dilution factors for different types of QD. Each type of QD has its own concentration for the maximum J_{sc}. The dilution factor 1× obtained the most satisfact-

ory results in 530-nm and 640-nm QDs, but the dilution factor 5× obtained the most satisfactory results in 460-nm QDs. According to this comparison, reflectance possibly dominated the outcome of J_{sc}, because the two curves are the most complimentary to each other among all three QDs. The importance of the LDS effect is yet to be verified.

The detailed current density versus voltage (J-V) characteristics of GaAs solar cells were determined at different dilution factors of 460-nm QDs, 530-nm QDs, 640-nm QDs, and without QDs by using a 100 mW/cm², AM1.5G spectrum simulator. The optimized photovoltaic J-V characteristics of the hybrid colloidal quantum-dot GaAs solar cells are shown in Fig. 5. The detailed electrical data is listed in Table 1. Dispensing a 530-nm QDs solution at a dilution factor of 1× onto the cell, the maximum short-circuit current density reached 22.87 mA/cm², and the power conversion efficiency increased from 14.48% to 18.05%, corresponding to a 24.65% enhancement, compared with a device without QDs. In addition, the open-circuit voltages (V_{oc}) of these devices exhibited no degradation, and the fill-factor (FF) remained at 77%. This evidence indicates that QDs on the surface of the GaAs solar cells did not interfere with diode operation. According to the measured data, all samples on which QD solution had been dispensed showed some degree of improvement when compared with the reference. Combined with the previous observation regarding reflectance profiles and J_{sc}, we believed a wavelength-dependent quantum efficiency measurement was necessary.

The spectral responses of EQE and surface reflectance were measured to further analyze the photon downshift and antireflection capability of QDs in GaAs solar cells as shown in Fig. 5(d)–(i). The combination of QDs and a GaAs solar cell exhibited a broad-range EQE enhancement from 300 to 900 nm. When we increased the QDs
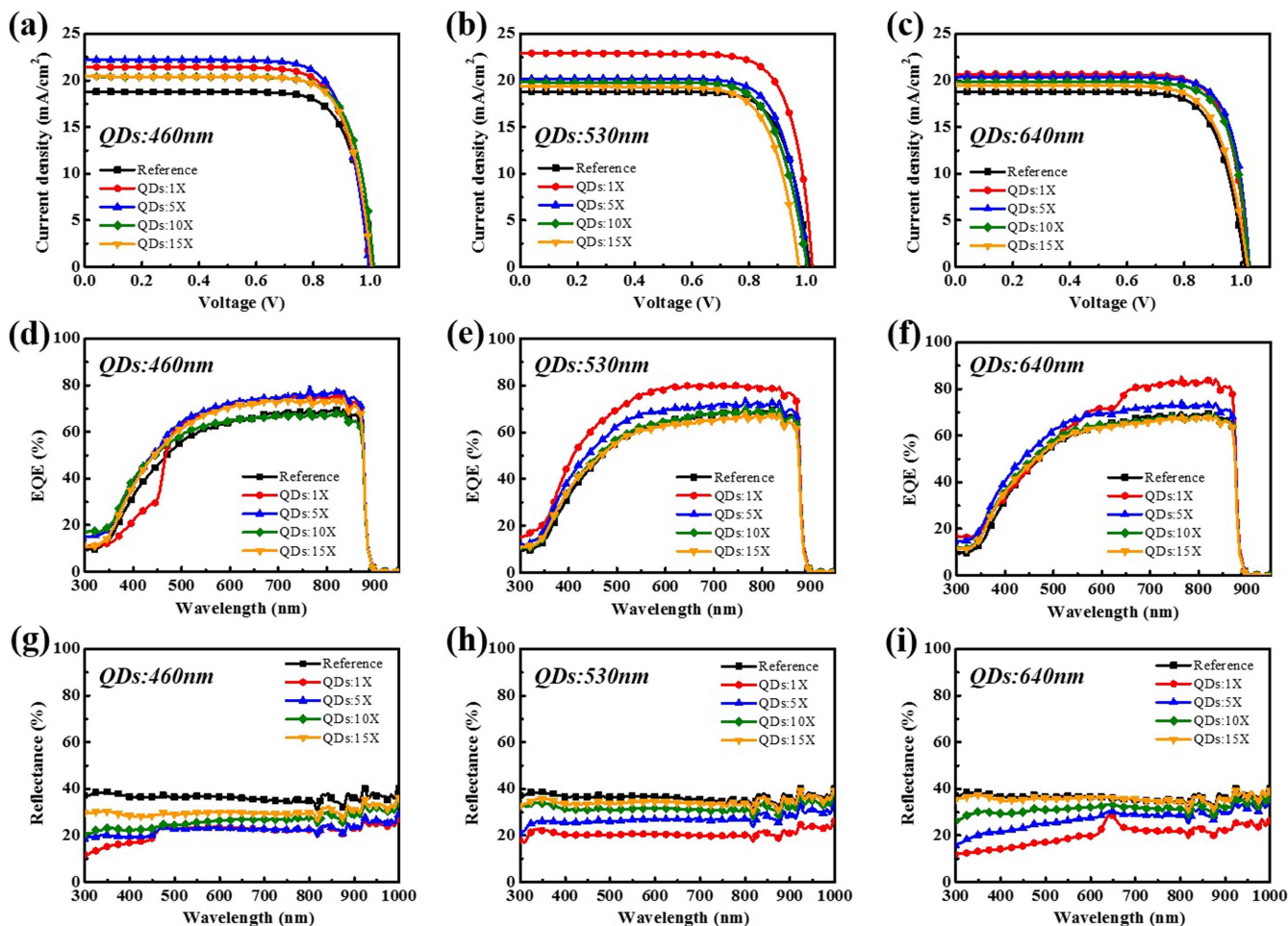
Figure 5 | Photovoltaic characteristics of GaAs solar cells with different type QDs and dilution factors. (a)–(c) the J-V characteristics; (d)–(f) the external quantum efficiencies; (g)–(i) surface reflectances of the 460-nm QDs, 530-nm QDs, and 640-nm QDs samples, respectively.

solution concentration, the broadband enhancement in the EQE curves became more obvious. Fig. 6 presents the calculated enhancement factors of EQE of QD dispensed cells with respect to the no-QDs reference cell, where the enhancement factor is defined as EQE_{QDs}/EQE_{ref}. To be more precise, the EQE of each sample is recorded before and after the QD dispense for the quantum efficiency enhancement analysis.

Discussion

Analysis on the internal quantum efficiency. Based on the Fig. 5, a change of surface reflectance occurs when QDs are dispensed onto GaAs cells. So there are two important factors in our scenario: anti-

Table 1 | The electrical characteristics of QD-hybrid GaAs solar cell

| Samples	V_{oc}(V)	J_{sc}(mA/cm²)	F.F (%)	Cell Efficiency (%)
Reference	1.01	18.76	76.27	14.48
QD460_1X	1	21.45	75.89	16.21
QD460_5X	0.99	22.21	76.34	16.85
QD460_10X	1.01	20.41	77.07	15.9
QD460_15X	1	20.41	77.24	15.79
Samples	V_{oc}(V)	J_{sc}(mA/cm²)	F.F (%)	Cell Efficiency (%)
Reference	1.01	18.76	76.27	14.48
QD530_1X	1.02	22.87	77.31	18.05
QD530_5X	1	20.17	76.35	15.47
QD530_10X	1	19.81	74.27	14.75
QD530_15X	0.97	19.34	74.64	14.06
Samples	V_{oc}(V)	J_{sc}(mA/cm²)	F.F (%)	Cell Efficiency (%)
Reference	1.01	18.76	76.27	14.48
QD640_1X	1.02	20.69	78.28	16.54
QD640_5X	1.03	20.38	79.71	16.69
QD640_10X	1.03	19.88	78.76	16.05
QD640_15X	1.02	19.46	75.52	15.01
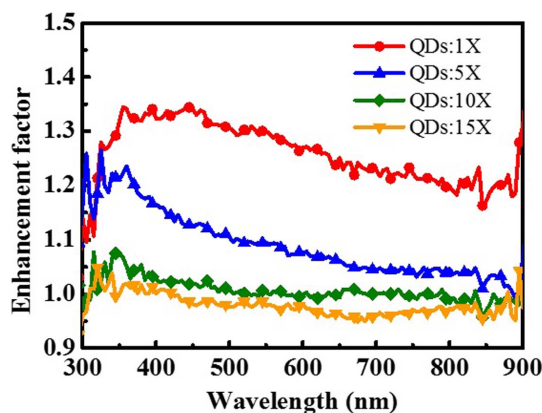
Figure 6 | (a) The measured external quantum efficiency results of GaAs solar cells with 530 nm QDs. (b) The enhancement factor of EQE between 530 nm QDs coated and no-QD coated devices.
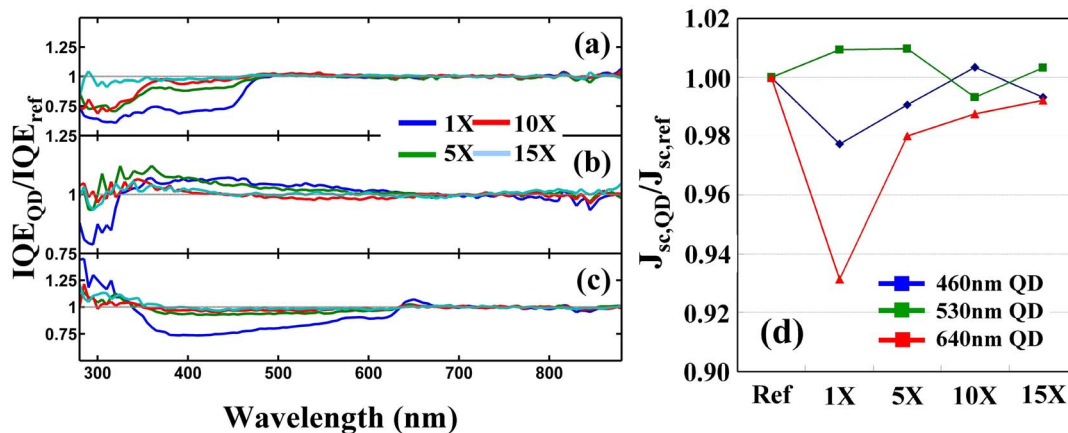
Figure 7 | (a)–(c) The IQE ratio between the QD samples and its reference. (a) 460 nm QD sample, (b) 530 nm QD sample, (c) 640 nm QD sample. (d) The calculated Jsc comparison based on the IQE obtained from Eq. 2.

reflection (AR) and LDS effects. In the UV range, this AR and the LDS effects are mingled together. While, in the spectrum where photon energy is below the band gap of QD, the LDS effect can be neglected. To properly characterize this, the AR effect, which is characterized by change of surface reflection, must be properly excluded. When the EQE is measured, the internal quantum efficiency (IQE) of the device is first multiplied by the $(1-R(\lambda))$ factor to count the transmitted photons correctly[37], where $R(\lambda)$ is the surface reflection spectrum. So the two quantities, EQE and IQE, share the connection as[37]:

$$IQE(\lambda) = \frac{EQE(\lambda)}{1-R(\lambda)} \qquad (2)$$

Thus, by dividing the EQE spectrum with the 1- $R(\lambda)$ and only considering IQE, the AR effect can be properly excluded. Comparison of the normalized IQE spectrum can reveal the possible enhancement or degradation of the device quantum efficiency internally. Fig. 7 (a) to (c) show the collection of the ratios of IQE with QDs to the pure GaAs IQE. A distinctive notch on the 460 nm and 640 nm QD IQE ratios at high concentration ($1\times$, no dilution case) indicates the strong absorption but weak re-emission capability of the QD under these conditions. The resultant cut into the quantum efficiency can deteriorate the overall performance. By integrating the IQE with solar spectrum, a no-AR effective J_{sc} can be obtained. This J_{sc} value when normalized by the reference GaAs J_{sc} can provide us a direct evaluation of the percentage of enhancement due to the LDS effect as shown in Fig. 7(d). From the plot, a 1% increase in 530 nm QD sample under original concentration and $5\times$ dilution can be found while

other colors like 460 nm and 640 nm ones shows less than 1 in almost all conditions, meaning no LDS effect in the device. From this point of view, the 530 nm QD performs better in promoting the LDS effect in the photovoltaic devices.

Evaluation of quantum dot LDS efficiency. From previous calculation of the internal quantum efficiency, the LDS effect from the QD layer can be revealed by excluding the AR effect from the EQE measurement. However, if the absorption of QD layer is strong but the re-emission rate is weak, any traces of QD luminescence can be "masked" and can not be seen, like the indentation we saw in Fig. 7. To probe further on the actual luminescent efficiency of the solid QD film, the absorption and the LDS efficiency have to be considered separately, and a diagram like Fig. 8 needs to be built for understanding the LDS mechanism. The LDS efficiency as we discuss here, can be defined as:

$$\eta_{LDS}(\lambda) = \frac{\text{\# of visible photons emitted}}{\text{\# of photons of wavelength } \lambda \text{ absorbed}} \qquad (3)$$

This η_{LDS} varies on the wavelength of the incident photons. When the incident photon energy is less than the QD band gap, the η_{LDS}

Figure 9 | **The corresponding absorption and η_{LDS} for (a) 460 nm QD and (b) 640 nm QD samples.** The measured single QD layer absorption (blue) and the calculated LDS efficiency(red) of the same device are shown in the plot. The light blue area marks the photon energy below the absorption edge, where there should be no η_{LDS}, and our calculation stops at the absorption edge. The dark lines of the η_{LDS} (at longer wavelengths than the absorption edges) are for visual guiding only.
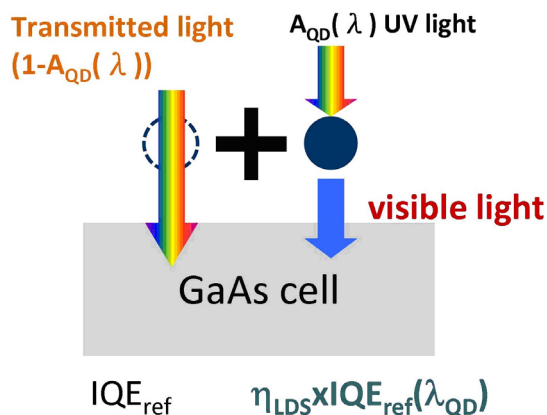

Figure 8 | Illustration of LDS effect: The detailed LDS mechanism between the incoming sunlight and re-emitted photons from QD layers.

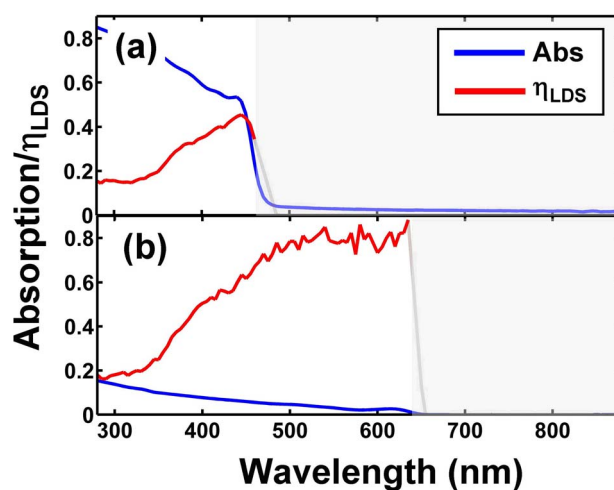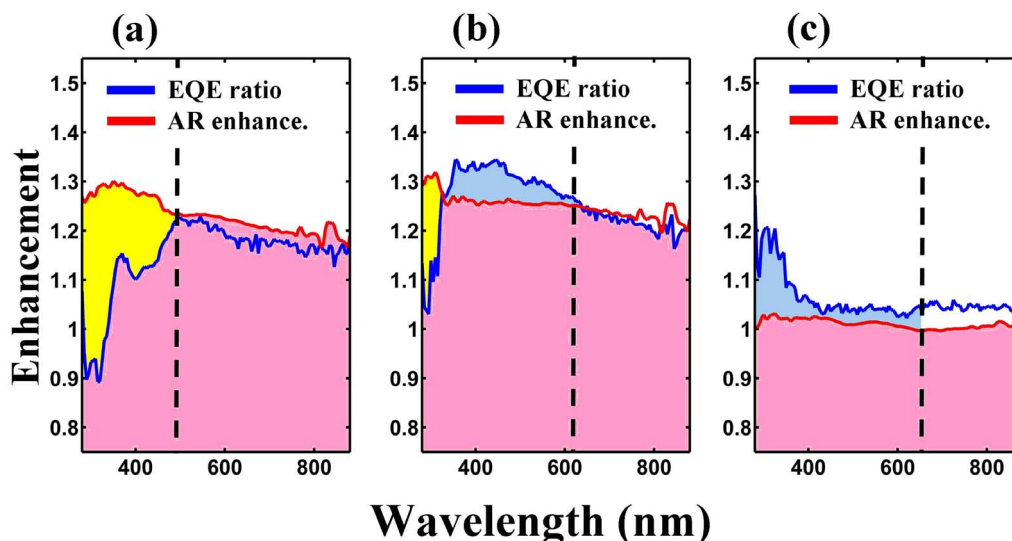**Figure 10** | The comparison curves of EQE enhancement and $(1 + \Delta_{AR})$, the AR enhancement, for (a) 460 nm QD, (b) 530 nm QD, (c) 640 nm QD. The pink colored area is the enhancement from the AR effect, while the blue area indicates the LDS enhancement. The yellow area is the absorption-dominated region when $(1 + \Delta_{AR})$ is higher than the EQE ratio.

becomes zero or negligible. In Fig. 8, certain non-ideal factors, such as total internal reflection, edge losses, and parasitic absorption, are not included in the current models. While we believe these are important and might be crucial to the completeness of the theory, the interaction between the LDS effect and AR effect could be dominant for the time being and should be considered first. A more thorough investigation on these non-ideal factors will be necessary to the future generation of the program. If these non-ideal factors are not considered, the IQE per unit wavelength has two components: one is from the photons penetrated through the QD layer, and the other is from the LDS effect. To formulate these two components, an expression can be written as:

$$IQE_{QD}(\lambda) = (1 - A_{QD}(\lambda))IQE_{ref}(\lambda) + \eta_{LDS}(\lambda) \times A_{QD}(\lambda) \times IQE_{ref}(\lambda_{QD}),$$
$$(4)$$

where $IQE_{QD}(\lambda)$ is the internal quantum efficiency of the whole device when QD layer is dispensed, A_{QD} is the absorption percentage of the QD layer, $IQE_{ref}(\lambda)$ is the internal quantum efficiency without the QD layer, and $IQE_{ref}(\lambda_{QD})$ is the efficiency at the QD emission peak. In this formula, the IQE is used to eliminate the surface reflection effect. Similar equations have been reported before[38,39]. In Eq. 4, the η_{LDS} (similar to the quantum yield of the quantum dots in solution) can be calculated once the absorption function A_{QD} and the quantum efficiency of the bare wafer are measured. The term, η_{LDS}, can then be found as:

$$\eta_{LDS}(\lambda) = \frac{IQE_{QD}(\lambda) - (1 - A_{QD}(\lambda)) \times IQE_{ref}(\lambda)}{A_{QD}(\lambda) \times IQE_{ref}(\lambda_{QD})} \quad (5)$$

The absorption data can be obtained from dispensing the same QD on the quartz glass slide and measuring the reflection and transmission before and after the dispense. The resultant LDS efficiencies for 460 nm and 640 nm QD are shown in Fig. 9 (a)

and (b). The η_{LDS} for 530 nm QD is, however, not realistic (>100%) due to the weak absorption of the QD exhibited in the measurement. The wavelength dependence of the η_{LDS} also confirmed that most of the emission should happen close to the absorption band edge since its maximum is always close to the band edge. The extracted peak η_{LDS} values are 45.5% for 460 nm QD and 88.1% for the 640 nm. In the meantime, the luminescent efficiency of the QD at UV region from the η_{LDS} spectrum is around 20% to 30%, which is close to the data provided by the vendor.

Enhancement factor evaluation. One question remains unanswered so far: how to define a suitable enhancement factor in this device? From the difference in the real world J_{sc}, one can only conclude that there are AR and LDS effects within, and it seems difficult to de-couple them. Deducing from definition of J_{sc}[37]:

$$\Delta J_{sc} = \int (\Delta EQE) \times F(\lambda) d\lambda$$
$$= \int \left(IQE_{QD}(1 - R_{QD}) - IQE_{ref}(1 - R_{ref}) \right) \times I_{AM1.5G}(\lambda) d\lambda$$
$$= \int \left(\frac{IQE_{QD}}{IQE_{ref}} \frac{1 - R_{QD}}{1 - R_{ref}} - 1 \right) \left(IQE_{ref}(1 - R_{ref}) \right) \times I_{AM1.5G}(\lambda) d\lambda$$
$$(6)$$
$$= \int \left(\frac{IQE_{QD}}{IQE_{ref}} \frac{1 - R_{QD}}{1 - R_{ref}} - 1 \right) \times EQE_{ref} \times I_{AM1.5G}(\lambda) d\lambda$$
$$= \int \left((1 + \Delta_{LDS})(1 + \Delta_{AR}) - 1 \right) \times EQE_{ref} \times I_{AM1.5G}(\lambda) d\lambda$$

A term $(1 + \Delta_{LDS})(1 + \Delta_{AR})$ emerges from the integral function, which can be defined as a wavelength dependent enhancement factor. In Eq. 6, the $(1 + \Delta_{LDS})$ is the ratio of IQE and the $(1 + \Delta_{AR})$ term is the ratio of $(1-R)$. This distributed enhancement should be more justifiable than a single number for one device. The overall

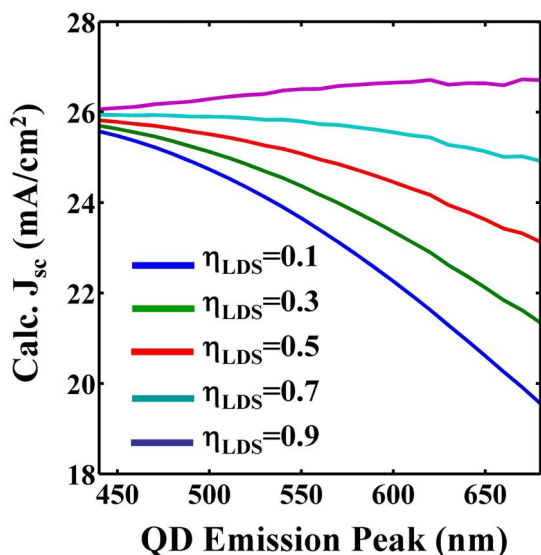| Table 2	The measured and calculated J_{sc} enhancement factors			
QD concentration	Measured $\Delta J_{sc}/J_{sc,ref}$	$\Delta J_{sc,AR}/J_{sc,ref}$	$\Delta J_{sc,LDS}/J_{sc,ref}$	Coupled term
QC530_1X	24.42%	24.28%	1.02%	0.27%
QD530_5X	6.14%	15.06%	1.08%	0.18%
QD530_10X	4.13%	6.71%	−0.62%	−0.05%
QD530_15X	2.23%	2.87%	0.33%	0.01%

6

Figure 11 | The calculated short-circuit current (J_{sc}) (based on Eq. 4) vs. different QD band gaps (emission peaks) of a hybrid QD-GaAs solar cell under different η_{LDS}. The QD absorption profile adapts the 460 nm QD's and adjust for corresponding QD band gaps.

enhancement, or can be named as "external" enhancement, is the ratio between EQE numbers. The relationship among these terms can be expressed as:

$$\frac{EQE_{QD}}{EQE_{ref}} = (1+\Delta_{LDS})(1+\Delta_{AR}) \qquad (7)$$

So in the Fig. 10, even though the external enhancement factor can be as high as 1.3 times, the final increase of the J_{sc} is lower than that peak value due to the solar spectrum weighted integration. Overlapping with the $(1 + \Delta_{AR})$ profile obtained from reflection spectrum can reveal if there is any LDS effect in the device. If the external enhancement is higher than the $(1 + \Delta_{AR})$ curve, the area in between them belongs to the LDS enhancement. However, if the external enhancement is close to or even lower than the $(1 + \Delta_{AR})$ curve, it is usually a clear indication of QD absorption take-over. Generally speaking, a peak (for good LDS effect) or a notch (for strong absorption of QD) can be found at UV region, while a close match between the $(1 + \Delta_{AR})$ curve and EQE ratio profile at long wavelengths can be expected, because the effects of LDS are negligible in this range, and only AR effect works in the longer range. While the enhancement factor of EQE is clearly defined as in Eq. 7, the enhancement factor of J_{sc} is more difficult to elucidate. To proceed further, we need to start from the Eq. 7:

$$\Delta J_{sc} = \int ((1+\Delta_{LDS})(1+\Delta_{AR})-1) \times EQE_{ref} \times I_{AM1.5G}(\lambda)d\lambda$$

$$= \int (\Delta_{AR} + \Delta_{LDS} + \Delta_{AR}\Delta_{LDS}) \times EQE_{ref} \times I_{AM1.5G}(\lambda)d\lambda \qquad (8)$$

$$= \Delta J_{sc,AR} + \Delta J_{sc,LDS} + \Delta J_{sc,coupled}$$

If the $\Delta J_{sc,coupled}$ term is small enough, the enhancement factor of Jsc can be regarded as the linear combination of the AR and LDS effect:

$$\frac{J_{sc,QD}}{J_{sc,ref}} = \frac{J_{sc,ref} + \Delta J_{sc}}{J_{sc,ref}} = 1 + \frac{\Delta J_{sc,AR} + \Delta J_{sc,LDS} + \Delta J_{sc,coupled}}{J_{sc,ref}}$$

$$\approx 1 + \frac{\Delta J_{sc,AR} + \Delta J_{sc,LDS}}{J_{sc,ref}} \qquad (9)$$

By using the definition in Eq. 8, the corresponding ΔJ_{sc} components can be calculated via the previously measured reflectance spectrum and the LDS effect from IQE. The calculated results, together with the measurement data, are listed in Table 2. The negative $\Delta J_{sc,LDS}$ represents no LDS enhancement at all. The coupled terms are generally small compared to the other two terms, which might validate Eq. 9. The best enhancement percentage on the J_{sc} by LDS effect happens at QD530_5X condition where a 1.08% of the reference J_{sc} is registered, and the AR effect takes another 15.06% of the $J_{sc,ref}$. If only the increased J_{sc} are counted, the LDS effect takes about 6% of the entire ΔJ_{sc}. Certain inconsistencies between the measured data and the calculated results are expected due to two reasons: first, there are some discrepancies between the light source in J-V measurement and the real solar spectrum, and the calculation in Eq. 8 uses the ideal AM1.5G spectrum. Second, there are possible errors in reflection measurement which cause deviations in the 1-R term of the Δ_{AR}.

To summarize for this matter, it is easy to define a clean enhancement factor in the EQE domain, however, the increment in J_{sc} is always the integral combination of the AR and LDS effect, which makes the definition of enhancement factor more obscure. We hope the definition in Eq. 8 can clarify this problem.

QD spectral dependence on J_{sc}. To investigate the QD emission wavelength dependence on the solar cell performance is the main topic of this work. In reality, however, a clean experiment is difficult to achieve. First, to cover the full visible spectrum with reasonable quantum yields, different types of QD structures (such as core-shell or bare) have to be used in the experiments. Second, the absorption strengths for different types of QDs are also different. Third, even though we could choose similar quantum yields in solution among different QDs, once they are dried on the GaAs surface, their final emission efficiency (i.e. η_{LDS}) might be very different as well. If we could assume an ideal condition, in which the absorption and η_{LDS} are all the same among different band gaps of quantum dots, then based on the Eq. 4, an IQE and the corresponding J_{sc} can be calculated across different QD emission wavelengths. First, a step-function like η_{LDS} is assumed, and the absorption edge, which is band gap of the QD, is the longest wavelength that gives η_{LDS} a non-zero and constant value. Other than that, if the excitation photonic energy is less than QD band gap, the η_{LDS} is zero. Second, the GaAs single junction solar cell is used for IQE. Third, the absorption spectra among different QDs are set to be the same shape as the one measured from 460 nm case, but only differ at the band gap wavelength (the onset of the absorption).

With these assumptions, the QD-emission-peak dependent J_{sc} can be calculated and graphed in Fig. 11 for different η_{LDS}. As can be observed from the plot, when QD is less efficient in LDS process (low η_{LDS}), we have to choose the blue QD to obtain high J_{sc}. Meanwhile, the high η_{LDS} can push the max J_{sc} towards longer wavelength choice

Table 3	The product information of the QDs			
QD in the paper	Product number	Product Description	PLQY by the vendor
QD400	662410	Lumidot™ CdS core-type quantum dots, 5 mg/mL in toluene	Not Available
QD460	662372	Lumidot™ CdS 460, core-type quantum dots, 5 mg/mL in toluene	Not Available
QD530	694649	Lumidot™ CdSe/ZnS 530, core-shell type quantum dots, 5 mg/mL in toluene	>=30%
QD560	694630	Lumidot™ CdSe/ZnS 560, core-shell type quantum dots, 5 mg/mL in toluene	>=30%
QD640	694606	Lumidot™ CdSe/ZnS 640, core-shell type quantum dots, 5 mg/mL in toluene	>=30%

Table 4 | The epitaxial layers of the single junction GaAs solar cells

Material	Thickness (nm)	Doping Type
GaAs	300	P+
$Al_{0.8}Ga_{0.2}As$	30	P
GaAs	200	P
GaAs	4000	N−
$Al_{0.3}Ga_{0.7}As$	120	N
GaAs	300	N
GaAs	Substrate	N

of QD band gap, which is close to the actual measured result in Fig. 4(a). In the mean time, the high η_{LDS} also help to increase the J_{sc} of the device. Although the situation will be largely different in the real world, this calculation echoes our measurement, and can provide a solid evaluation in terms of choosing suitable QDs for photovoltaic enhancement purpose.

Conclusion

In conclusion, we examined the different responses of hybrid solar cells according to the emission wavelengths of top QD layers. Among the QD samples, the green QD exhibited the most satisfactory enhancement. A QD layer considerably enhanced short-circuit current density and power conversion efficiency at AM1.5G. The enhancement can mainly be attributed to the photon downshift effect and antireflection. The enhanced short-circuit currents and weighted reflectance were evaluated using different dilution factors of QD solutions to determine the optimal condition. After the optimal condition was determined, the optimized PCE was enhanced by 24.65% when compared to cells without a QDs layer. In the EQE spectral response, a 1.3-fold enhancement was observed between the QDs and the reference samples. Finally, the LDS and antireflection capability were analyzed quantitatively using absorption and EQE enhancement curves. We believe this technology is a great candidate for use in the next generation of highly efficient photovoltaic devices in the near future.

Methods

Equipment set up. The power conversion efficiencies of GaAs solar cells were measured using a procedure complying with the international standard CEI IEC 60904-1. The J-V measurement system consisted of a power supply (Newport 69920), a 1000-W Class-A solar simulator (Newport 91192A) with a Xenon lamp (Newport 6271A) and an Air Mass 1.5, Global (AM1.5G) illumination filter (Newport 81088A), a probe stage, and a source meter with a 4-wire mode (Keithley 2400). Class-A Air Mass 1.5, Global (AM1.5G) illumination at a power of 1000 W/m^2 was used to characterize all of the solar cells in our experiment[16]. The testing chuck was thermally stabilized by circulating water through temperature controlled chiller system, and the temperature is controlled within 25 ± 1°C. After calibration by the Newport Corporation, our light source showed only 0.88% temporal instability and 0.79% light intensity nonuniformity. To determine the status of the light source during every measurement, the measurements of the instruments were double-checked. The spectrum of the solar simulator was measured using a calibrated spectrometer (Soma S-2440) in the wavelength range 300–1100 nm, and the intensity of the solar simulator was calibrated using a monocrystalline silicon reference cell with a 4 cm^2 illumination area (VLSI Standards, Inc.)[40].

The light source of the external quantum efficiency (EQE) measurement system consisted of a 300-W Xenon lamp (Newport 66984) and a monochromator (Newprot 74112). The beam spot on the sample was rectangular, and the spot size was roughly 3 mm^2. Spectrum calibration was conducted using a calibrated silicon photodetector with a reported spectral response (Newport 818-UV). To convert the photocurrent of the sample to the voltage signal, a preamplifier (Princeton Applied Research, Model 181) was used, and the magnifying signal was imported into the lock-in amplifier. The EQE measurement was taken using a lock-in amplifier (Standard Research System, SR830), and an optical chopper unit (SR540) operating at a 260 Hz chopping frequency. The temperatures of the cells were controlled using the same method used for the J-V measurements[36,41].

Colloidal quantum dot information. In this section, the detailed quantum dots information will be provided. The QD solutions used in this paper were purchased from Sigma-Aldrich Corporation. The average diameter of 460-nm QDs, 530-nm QDs and 640-nm QDs were approximately 5 nm, 6 nm and 8 nm, respectively. The product numbers for these QDs are listed in Table 3.

GaAs solar cell preparation. The GaAs solar cells were purchased from Millennium Communications Co. Ltd., and the product number is SC-006-01. The typical epitaxial structure is shown in Table 4 (provided by manufacturer).

The typical electrical characteristics of the AR coated devices are: V_{oc} = 0.93 V, J_{sc} = 26 mA/cm^2, power conversion efficiency = 21 ± 3%.

The devices under test were not AR-coated and selected from a pool of GaAs solar cell chips. The J_{sc} and EQE were the key parameters to be inspected. The average J_{sc} is 18.87 mA and the standard deviation among these samples is 0.125 mA, which stands for about 0.66% variation across the chips. Their EQEs were also closely matched. The GaAs solar cell is 1 cm by 1 cm square shape.

Quantum dot dispense. We dispense the QD solution onto the chip by micropipette (Manufacturer: Dragon Lab, Micropette pipette). Usually the process steps are like:

1. clean the chips with solvent (such as acetone, IPA).
2. Use water bath to ultrasound the QD solution for 5 minutes.
3. If dilution is needed, draw certain volume of ultra-sounded solution and add proper quantity of toluene to the QD solution, and then another 5 minutes of ultrasound to mix the particles completely. The original concentration of QD is 5 mg/mL, and the dilution is based on this number and adding the corresponding volume of toluene.
4. Use micropipette to draw all the solution and manually drop the QD solution on the chip evenly.
5. Leave the chip to air-dry the fume hood.

After the dry-up, the quantum dots become solid-phase patches in 100–500 nm size. The aggregation of the QDs could be detected via the PL spectrum in the solution and after solidification on the surface. A red-shifted peak was observed and the amount of shift is 12.6 meV (or 2.164 nm), which indicates possible aggregation of the dried QDs. From the TEM inspection shown in Fig. 3(c), no ordered structure can be found in our dispensed layer.

1. Kayes, B. M. *et al.* 27.6% Conversion efficiency, a new record for single-junction solar cells under 1 sun illumination. *37th IEEE Photovoltaic Specialists Conference (PVSC).* ((doi:10.1109/PVSC.2011.6185831) (2011).
2. Green, M. A., Emery, K., Hishikawa, Y., Warta, W. & Dunlop, E. D. Solar cell efficiency tables (version 41). *Prog. Photovoltaics* **21**, 1–11; doi:10.1002/pip.2352 (2013).
3. Polman, A. & Atwater, H. A. Photonic design principles for ultrahigh-efficiency photovoltaics. *Nat. Mater.* **11**, 174–177 (2012).
4. Miller, O. D., Yablonovitch, E. & Kurtz, S. R. Strong Internal and External Luminescence as Solar Cells Approach the Shockley–Queisser Limit. *IEEE J Photovoltaics* **2**, 303–311; doi:10.1109/JPHOTOV.2012.2198434 (2012).
5. Chhajed, S., Schubert, M., Kim, J. & Schubert, E. Nanostructured multilayer graded-index antireflection coating for Si solar cells with broadband and omnidirectional characteristics. *Appl. Phys. Lett.* **93**, 251108 (2008).
6. Tsai, M. A., Tseng, P. C., Chen, H. C., Kuo, H. C. & Yu, P. C. Enhanced conversion efficiency of a crystalline silicon solar cell with frustum nanorod arrays. *Opt. Express* **19**, A28–A34; doi:10.1364/oe.19.000a28 (2011).
7. Richards, B. S. Luminescent layers for enhanced silicon solar cell performance: Down-conversion. *Sol. Energy Mater. Sol. Cells* **90**, 1189–1207; doi:http://dx.doi.org/10.1016/j.solmat.2005.07.001 (2006).
8. Hovel, H. J., Hodgson, R. T. & Woodall, J. M. The effect of fluorescent wavelength shifting on solar cell spectral response. *Solar Energy Materials* **2**, 19–29; doi:http://dx.doi.org/10.1016/0165-1633(79)90027-3 (1979).
9. McIntosh, K. R. *et al.* Increase in External Quantum Efficiency of Encapsulated Silicon Solar Cells from a Luminescent Down-Shifting layer. *Prog. Photovoltaics* **17**, 191–197; doi:10.1002/pip.867 (2009).
10. Klampaftis, E. & Richards, B. S. Improvement in multi-crystalline silicon solar cell efficiency via addition of luminescent material to EVA encapsulation layer. *Prog. Photovoltaics* **19**, 345–351; doi:10.1002/pip.1019 (2011).
11. Klampaftis, E., Ross, D., McIntosh, K. R. & Richards, B. S. Enhancing the performance of solar cells via luminescent down-shifting of the incident spectrum: A review. *Sol. Energy Mater. Sol. Cells* **93**, 1182–1194; doi:10.1016/j.solmat.2009.02.020 (2009).
12. Rowan, B. C., Wilson, L. R. & Richards, B. S. Advanced material concepts for luminescent solar concentrators. *IEEE J. Sel. Topics Quantum Electron.* **14**, 1312–1322 (2008).
13. Sah, R., Baur, G. & Kelker, H. Influence of the solvent matrix on the overlapping of the absorption and emission bands of solute fluorescent dyes. *Appl. Phys.* **23**, 369–372 (1980).
14. Chen, H.-C. *et al.* Enhanced efficiency for c-Si solar cell with nanopillar array via quantum dots layers. *Opt. Express* **19**, A1141–A1147 (2011).
15. Lin, C.-C. *et al.* Highly efficient CdS-quantum-dot-sensitized GaAs solar cells. *Opt. Express* **20**, A319–A326 (2012).
16. Chen, H.-C. *et al.* Enhancement of power conversion efficiency in GaAs solar cells with dual-layer quantum dots using flexible PDMS film. *Sol. Energy Mater. Sol. Cells* **104**, 92–96; doi:10.1016/j.solmat.2012.05.003 (2012).
17. Cheng, Z. J., Su, F. F., Pan, L. K., Cao, M. & Sun, Z. CdS quantum dot-embedded silica film as luminescent down-shifting layer for crystalline Si solar cells. *J. Alloys Compd.* **494**, L7–L10; doi:10.1016/j.jallcom.2010.01.047 (2010).

18. Pi, X. D., Zhang, L. & Yang, D. R. Enhancing the Efficiency of Multicrystalline Silicon Solar Cells by the Inkjet Printing of Silicon-Quantum-Dot Ink. *J. Phys. Chem. C* **116**, 21240–21243; doi:10.1021/jp307078g (2012).

19. Hodgson, S. D., Brooks, W. S. M., Clayton, A. J., Kartopu, G., Barrioz, V. & Irvine, S. J. C. Enhancing blue photoresponse in CdTe photovoltaics by luminescent down-shifting using semiconductor quantum dot/PMMA films. *Nano Energy* **2**, 21–27; doi:10.1016/j.nanoen.2012.07.006 (2013).

20. Goetzberger, A. & Greube, W. Solar energy conversion with fluorescent collectors. *Appl. Phys.* **14**, 123–139; doi:10.1007/BF00883080 (1977).

21. Klampaftis, E., Ross, D., Seyrling, S., Tiwari, A. N. & Richards, B. S. Increase in short-wavelength response of encapsulated CIGS devices by doping the encapsulation layer with luminescent material. *Sol. Energy Mater. Sol. Cells* **101**, 62–67 (2012).

22. Ross, D., Klampaftis, E., Fritsche, J., Bauer, M. & Richards, B. S. Increased short-circuit current density of production line CdTe mini-module through luminescent down-shifting. *Sol. Energy Mater. Sol. Cells* **103**, 11–16; doi:10.1016/j.solmat.2012.04.009 (2012).

23. Glaeser, G. C. & Rau, U. Improvement of photon collection in Cu(In,Ga)Se2 solar cells and modules by fluorescent frequency conversion. *Thin Solid Films* **515**, 5964–5967 (2007).

24. Maruyama, T., Enomoto, A. & Shirasawa, K. Solar cell module colored with fluorescent plate. *Sol. Energy Mater. Sol. Cells* **64**, 269–278 (2000).

25. Peng, M. *et al*. Integration of fiber dye-sensitized solar cells with luminescent solar concentrators for high power output. *Journal of Materials Chemistry A* **2**, 926–932 (2014).

26. Grätzel, M. Dye-sensitized solar cells. *Journal of Photochemistry and Photobiology C: Photochemistry Reviews* **4**, 145–153 (2003).

27. Kongkanand, A., Tvrdy, K., Takechi, K., Kuno, M. & Kamat, P. V. Quantum dot solar cells. Tuning photoresponse through size and shape control of CdSe-TiO2 architecture. *J. Am. Chem. Soc.* **130**, 4007–4015 (2008).

28. Nozik, A. Quantum dot solar cells. *Physica E: Low-dimensional Systems and Nanostructures* **14**, 115–120 (2002).

29. Gardelis, S. & Nassiopoulou, A. G. Evidence of significant down-conversion in a Si-based solar cell using CuInS2/ZnS core shell quantum dots. *Appl. Phys. Lett.* **104**, 183902 (2014).

30. Kalytchuk, S. *et al*. Semiconductor Nanocrystals as Luminescent Down-Shifting Layers To Enhance the Efficiency of Thin-Film CdTe/CdS and Crystalline Si Solar Cells. *The Journal of Physical Chemistry C*; DOI: 10.1021/jp410279z (2014). Publication Date: January 17, 2014.

31. Hodgson, S. D. *et al*. Increased conversion efficiency in cadmium telluride photovoltaics by luminescent downshifting with quantum dot/poly (methyl methacrylate) films. *Prog. Photovoltaics*; DOI: 10.1002/pip.2408 (2013). Publication Date: August 6, 2013.

32. Sigma-Aldrich Co. LLC, *Aldrich Materials Science*, (2014), Date of access: 11/06/2014, http://www.sigmaaldrich.com/materials-science.html.

33. Schubert, E. F. Refractive index and extinction coefficient of materials, (2004), Date of access: 11/06/2014, http://homepages.rpi.edu/~schubert/Educational-resources/Materials-Refractive-index-and-extinction-coefficient.pdf.

34. Hanrahan, P. & Krueger, W. Reflection from layered surfaces due to subsurface scattering. *Proceedings of the 20th annual conference on Computer graphics and interactive techniques*. (1993).(ACM).

35. Tseng, P.-C. *et al*. Enhanced omnidirectional photon coupling via quasi-periodic patterning of indium-tin-oxide for organic thin-film solar cells. *Org. Electron.* **12**, 886–890 (2011).

36. Tseng, P. C. *et al*. Angle-resolved characteristics of silicon photovoltaics with passivated conical-frustum nanostructures. *Sol. Energy Mater. Sol. Cells* **95**, 2610–2615; doi:10.1016/j.solmat.2011.05.010 (2011).

37. Sze, S. M. & Ng, K. K. *Physics of semiconductor devices*. (John Wiley & Sons, 2006).

38. Van Sark, W., Meijerink, A., Schropp, R., Van Roosmalen, J. & Lysen, E. Enhancing solar cell efficiency by using spectral converters. *Sol. Energy Mater. Sol. Cells* **87**, 395–409 (2005).

39. Geyer, S. M., Scherer, J. M., Moloto, N., Jaworski, F. B. & Bawendi, M. G. Efficient luminescent down-shifting detectors based on colloidal quantum dots for dual-band detection applications. *ACS nano* **5**, 5566–5571 (2011).

40. Emery, K. A. & Osterwald, C. R. Solar-Cell Calibration Methods. *Solar Cells* **27**, 445–453; doi:10.1016/0379-6787(89)90054-9 (1989).

41. Smestad, G. P. *et al*. Reporting solar cell efficiencies in solar energy materials and solar cells. *Sol. Energy Mater. Sol. Cells* **92**, 371–373; doi:10.1016/j.solmat.2008.01.003 (2008).

Acknowledgments

Author contributions

H.V.H., C.C.L., H.C.C. and K.J.C. designed the experiments. H.V.H. and C.C.L. analyzed the results and wrote the manuscript. C.C.L., H.C.K. and P.Y. suggested the study and led the project. Y.L.T. carried out SEM measurement. H.V.H., Y.L.Y. and W.Y.L. characterized the materials and devices. All authors discussed about the results and commented on the manuscript.

Additional information

Competing financial interests: The authors declare no competing financial interests.

How to cite this article: Han, H.-V. *et al*. A Highly Efficient Hybrid GaAs Solar Cell Based on Colloidal-Quantum-Dot-Sensitization. *Sci. Rep.* **4**, 5734; DOI:10.1038/srep05734 (2014).